



Epitaxial Growth of Ag on Au(111) by Galvanic Displacement of Pb and Tl Monolayers

R. Vasilic,^{a,*} L. T. Viyannalage,^b and N. Dimitrov^{a,b,**,z}

^aMaterials Science and Engineering Program, and ^bDepartment of Chemistry, State University of New York at Binghamton, Binghamton, New York 13902, USA

The development of a new method for epitaxial growth of metals in solution by galvanic displacement of layers predeposited by underpotential deposition (UPD) is discussed and experimentally illustrated. Cyclic voltammetry and scanning tunneling microscopy are employed to carry out and monitor a “quasi-perfect,” two-dimensional growth of up to 35 monolayers of Ag on Au(111) by repetitive galvanic displacement of underpotentially deposited Tl and Pb monolayers. A complementary kinetic study of Pb and Tl UPD layer stability at open-circuit potential identifies the oxygen reduction reaction and hydrogen evolution reaction as key oxidative competitors of Ag in the proposed displacement protocol. Analysis of the morphology evolution during the growth of Ag by displacement Pb and Tl UPD layers suggests the one-to-one exchange scenario (Ag–Tl) as more efficient for longer maintenance of a layer-by-layer silver deposition. The excellent quality of layers deposited by monolayer-restricted galvanic displacement is manifested by a steady UPD voltammetry and ascertained by an overall flat and uniform surface morphology maintained during the entire growth process. An X-ray photoelectron spectroscopy analysis finds no traces of Pb and Tl in the Ag deposit. © 2006 The Electrochemical Society. [DOI: 10.1149/1.2218769] All rights reserved.

Manuscript submitted April 4, 2006; revised manuscript received May 8, 2006. Available electronically July 13, 2006.

The growth of smooth, homo-, and heteroepitaxial metal layers has always been a major goal of electrodeposition. Such layers are considered superior to any other kind of thin films as they strictly reproduce the crystallography and (in general) the morphology of the underlying substrate surface. Epitaxial metallic layers also feature reduced ohmic resistivity and electromigration that, along with their continuity, render these layers highly desirable for applications in the electronics industry and in the synthesis of low-metal loading catalysts.

Thin-film growth modes are generally classified as Frank–van der Merve or layer-by-layer (2D) growth, Volmer–Weber or 3D-cluster growth, and Stranski–Krastranov (SK) mode, the latter associated with a transition from 2D to 3D growth.¹ Step-flow growth is a multilayer variant of Frank–van der Merve mode and occurs at an appropriate step density and deposition flux. As long as 2D mode is operating during the growth (whether monolayer or multilayer), the resulting film is in registry with the substrate structure. However, the vast majority of characterized heteroepitaxial systems displays either 3D or SK growth mode at ambient temperature. In addition, owing to kinetic issues, 3D growth is often encountered even in overlayer/substrate systems that should, according to thermodynamic considerations, grow in a flat, 2D mode. As a result, 3D clusters that are far apart grow predominantly in the vertical direction to merge eventually at a considerable layer thickness in a polycrystalline metal deposit.

A major advance toward electrodeposition of smooth, epitaxial metal deposits was made by Sieradzki et al. with the development of defect mediated growth (DMG)² and surfactant mediated growth (SMG).³ The protocols employed in these techniques assume either codeposition of the growing metal with a reversibly deposited mediator metal (Pb²⁺ or Cu²⁺) (DMG) or use a predeposited submonolayer of “surfactant” metal (Pb²⁺) (SMG) that floats on the top of the depositing metal and facilitates the 2D growth in the system of interest. The applicability of these methods was successfully demonstrated by growth of commercially thick metal deposits in the systems Ag/Au(111), Ag/Ag(111),^{2,3} and Cu/Au(111)⁴ with Pb²⁺ or Cu²⁺ as mediators. Recent X-ray specular reflectivity measurements of Wang et al.⁵ demonstrated that nearly complete (“perfect 2D”) monolayer (ML) and bilayer Ag films can be grown by optimized DMG procedures.

Although results of structural characterization and elemental analysis suggest smooth and inclusion-free epitaxial films grown by

DMG and SMG,^{2–4} these methods are still subject to some limitations and practical inconvenience that need to be addressed. For instance, both methods are tunable over a variety of parameters, including metal concentrations, scan rate, potential limits, and submonolayer coverage that are mutually dependent and thus difficult to balance. Also, the thickness control (via charge measurements) during growth is hindered by the interference of factors such as side reactions and double-layer charging that, especially in DMG, are manifested by currents comparable to (or even exceeding) the deposition current level. Finally, although very low, the possibility for incorporation of mediator into the deposit cannot be completely ruled out.

In this paper we present an electrochemical and scanning tunneling microscopy (STM) study aimed at experimental validation of a recently proposed deposition method⁶ realizing a monolayer-restricted galvanic displacement (GD) as a “building block” for the growth of smooth, epitaxial metal films. The employed strategy utilizes a concept first proposed and then widely used for submonolayer to monolayer surface modification, assisted by irreversible galvanic displacement of underpotentially predeposited less-noble metal by a more-noble metal of interest.^{7,8} The newly developed protocol is enabled for heteroepitaxial systems in which the displaced metal deposits underpotentially not only on the substrate, but also on the growing metal, so that the “building block” reaction may be repeated as many times as desired. Similarly, repetitive deposition loops have been technically used for years in electrochemical atomic layer epitaxy (EC ALE) for growth of epitaxial, compound semiconductor layers with wide application in the electronics industry.⁹ Recent proof-of-concept results demonstrated excellent growth uniformity achieved by multiple application of a galvanic displacement step.⁶ A perfect thickness control during the deposition is warranted by the redox exchange stoichiometry. The electroless nature of the displacement reaction enables the decoupling of mutually dependent in a typical DMG or SMG scenario, growth controlling factors thus improving the overall deposition control. Lastly, a potential monitoring during the displacement reaction serves to virtually exclude incorporation of the UPD metal into the growing layer.

In this work the growth experiments are preceded by a concise kinetic study of the stability of Tl and Pb UPD layers on Ag(111) at open-circuit potential (OCP). This effort is justified by arguments (discussed in more detail elsewhere¹⁰) associated with the competition between Ag⁺ as displacing ions and oxidative agents such as oxygen reduction reaction (ORR) and hydrogen evolution reaction (HER). The ultimate goal of these experiments is to determine quantitatively a concentration of Ag⁺ that will guarantee maximum efficiency and thus a stoichiometric yield of the employed displacement

* Electrochemical Society Student Member.

** Electrochemical Society Active Member.

^z E-mail: dimitrov@binghamton.edu

strategy. In the deposition part of this work we have chosen as a prototype the growth of Ag on Au(111). In particular, a repetitive displacement of a predeposited Pb UPD layer by silver ions serves as a building block reaction. Without displacement, or additional kinetics manipulation, the Ag/Au(111) system grows in an SK mode, forming two wetting layers prior to 3D cluster formation.¹¹ This identifies Ag/Au(111) as an excellent candidate for implementation of protocols that would facilitate and help maintain 2D growth to a considerable thickness of the resulting layer. Another advantage of that system is the well-documented ability of Tl and Pb to deposit underpotentially on Au(111) and Ag(111)¹²⁻¹⁶ featuring distinct voltammetric behavior that allows for quantitative discrimination between silver and gold substrates.¹⁷

Experimental

Kinetic experiments (stability of UPD layers at OCP).—A (111)-oriented silver crystal (Monocrystals Co.), 3 mm thick and 1 cm in diameter, was prepared using a modified procedure originally described in Ref. 18. First, the crystal was mechanically polished with water-based deagglomerated alumina suspensions (Buehler) down to 0.05 μm and rinsed with water. In the next step Ag crystal was kept in concentrated H_2SO_4 for 5–10 min and subsequently rinsed with Barnstead Nanopure ($>18.3 \text{ M}\Omega$) and dried in nitrogen. Then, it was transferred to 4 M CrO_3 + 0.6 M HCl chemical polishing solution. The chemical polishing took place (usually for 10–15 s) until the Ag surface was uniformly covered with yellow-orange oxide film. Afterward, the crystal was rinsed with Barnstead Nanopure water and soaked in concentrated NH_3 to completely remove the oxide film. This step was followed by rinsing with Nanopure water and subsequent immersion in concentrated H_2SO_4 for additional 5 min to dissolve any oxide remnants on the crystal surface. After a final rinsing, the crystal was transferred to the electrochemical cell under the protection of deoxygenated water droplet. During the experiments the Ag(111) crystal was held in contact with the solution through a hanging meniscus configuration.¹⁹ The UPD layer stability at OCP was investigated by chronopotentiometry in Tl^+ and Pb^{2+} perchlorate-based solutions with controlled pH and oxygen content. A PAR-273 potentiostat coupled with a Nicolet 310 digital storage oscilloscope was used to record chronopotentiograms at OCP and to measure steady-state reduction currents prior to each experiment.

Growth experiments (galvanic displacement).—A mechanically polished, electropolished, and flame annealed Au(111) single-crystal (Monocrystals Co.), 2 mm thick and 1 cm in diameter, was used as a working electrode (WE). The mechanical polishing down to 0.05 μm was done using water-based, deagglomerated alumina suspensions (Buehler). The gold surface was then electropolished by anodization in 3:2:1 ethylene glycol, hydrochloric acid, and glacial acetic acid for 10–15 s at a dc current density of 2.5 A cm^{-2} with a platinum cathode. After a thorough rinsing with Barnstead Nanopure water ($>18 \text{ M}\Omega$) the Au crystal was annealed to red heat in a propane flame for 10 min and cooled rapidly in nitrogen atmosphere. The surface was terminated by a water droplet to prevent contamination and mounted on a holder for work at a hanging meniscus configuration.¹⁹ Finally, the holder with the crystal was placed in a state-of-the-art, controlled environment, three-compartment electrochemical setup, which allows for multiple electrolyte immersion of the WE.⁶ In this setup, a static, quartz glass Petri dish containing $1 \times 10^{-1} \text{ M NaClO}_4 + 1 \times 10^{-2} \text{ M HClO}_4 + 3 \times 10^{-3} \text{ M Pb}(\text{ClO}_4)_2$ [or $5 \times 10^{-3} \text{ M TiClO}_4$ instead of $\text{Pb}(\text{ClO}_4)_2$] solution serves as a three-electrode cell where UPD experiments are carried out using a Pb wire [or mercury sulfate electrode (MSE) in the case of Tl] as a reference electrode and a Pt wire serving as a counter electrode. Two other quartz glass compartments, containing, respectively, $1 \times 10^{-2} \text{ M AgClO}_4 + 1 \times 10^{-2} \text{ M HClO}_4$ solution for the galvanic displacement, and Barnstead Nanopure water for rinsing, are mounted on a turret assembly.

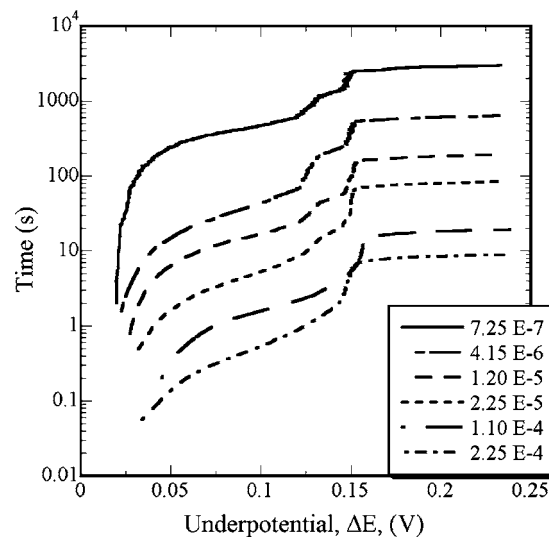


Figure 1. OCP transients illustrating the dependence of the Pb UPD layer stability upon the oxygen concentration in $3 \times 10^{-3} \text{ M Pb}(\text{ClO}_4)_2 + 1 \times 10^{-2} \text{ M HClO}_4 + 1 \times 10^{-1} \text{ M NaClO}_4$ solution. Inset legend: oxygen concentration (mol L^{-1}) prior to each transient registration.

A vertical mobility of the WE holder and an in-plane rotation of the turret platform operated by an accessible shaft enable the multiple solution immersion of the WE. All three compartments are incorporated in a clear acrylic jar with a sealable lid, equipped with purging ultrahigh-purity (UHP) nitrogen gas connections for oxygen evacuation. Cyclic voltammetry experiments were performed with a Cypress Systems 66-OMNI-101B potentiostat equipped with the 66-Acquire101 software package to collect experimental data on a computer. All solutions were made with highest purity grade chemicals and Barnstead Nanopure water. For the sake of clarity, all potentials are quoted as underpotentials ΔE , ($\Delta E = E - E_{\text{Me}^{z+}/\text{Me}}$, and E is the applied potential). MSE is used for potential reference where underpotential cannot be defined (Fig. 3—two UPD metals and Fig. 10—no UPD metal).

Characterization experiments (STM and XPS).—After the growth, the Au crystal with the deposited Ag layer was rinsed with Nanopure water and transferred with a small water droplet to an environmental chamber steadily purged with UHP nitrogen, where ex situ STM experiments were performed. A molecular imaging (MI) Pico Scan 300S scanner, MI Pico Scan 2100 controller, and MI Pico Scan software were used for monitoring the Ag layer surface morphology. Tips for the STM experiments were made by etching of Pt 80%–Ir 20% wire in a 1:2 mixture of saturated CaCl_2 solution and water at 25 V (ac).

X-ray photoelectron spectroscopy (XPS) experiments were carried out at the Center for Nanoscale Systems (CNS) at Cornell University. The instrument used was Surface Science SSX-100 [X-ray source—Al $\text{K}\alpha$ (1486.6 eV)] spectrometer operating at base pressure of 1×10^{-9} Torr with both incident beam and detector angle set to 55° . The spot size was 1000 μm .

Results and Discussion

Kinetic study: stability of Pb and Tl UPD layers at OCP.—The influence of dissolved oxygen on the Pb UPD layer stability at OCP was investigated by chronopotentiometry according to an experimental protocol described elsewhere.¹⁰ Figure 1 represents potential-time dependences obtained in $2 \times 10^{-4} \text{ M Pb}(\text{ClO}_4)_2 + 1 \times 10^{-2} \text{ M HClO}_4 + 1 \times 10^{-1} \text{ M NaClO}_4$ solution after different times of solution deoxygenation. The oxygen concentrations summarized in the legend of Fig. 1 are calculated based on a measurement of steady-state current densities at the initial potential prior

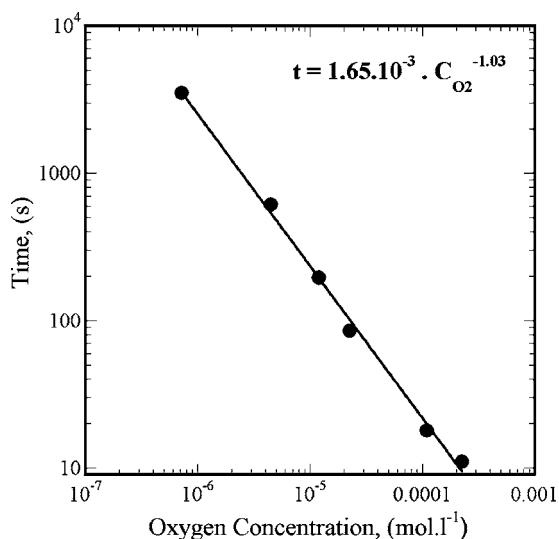


Figure 2. Dependence of the time to strip a Pb monolayer (measured at the flat part of the curves in Fig. 1) upon the oxygen concentration in 3×10^{-3} M $\text{Pb}(\text{ClO}_4)_2 + 1 \times 10^{-2}$ M $\text{HClO}_4 + 1 \times 10^{-1}$ M NaClO_4 solution. The inset equation shows linear regression parameters.

to each chronopotentiometric experiment. Assuming a diffusion-controlled ORR on a Pb covered Ag(111) in perchlorate solution over the entire oxygen concentration range²⁰ one can attribute a particular O_2 concentration to each current value using the linear dependence

$$i_{\text{lim}} = k \times C_{\text{O}_2} \quad [1]$$

where i_{lim} is the oxygen diffusion-limited current density, k is a constant of proportionality, and C_{O_2} is the bulk oxygen concentration. A relevant reference number to quantify the proportionality in Eq. 1 is the bulk concentration of O_2 in naturally aerated solution, $C_{\text{O}_2} = 2.25 \times 10^{-4}$ mol L^{-1} .²¹ The chronopotentiometric experiments were initiated at underpotential of 0.03 V by taking off the potential control. The nitrogen purging was discontinued during the registration of each transient and the cell was kept hermetically closed to assure steady experimental conditions. The curves plotted in Fig. 1 illustrate a strong dependence of the UPD layer stability upon the presence of O_2 in the solution. It is clear that the UPD layer stripping time, t_{str} , increases up to three orders of magnitude as the oxygen concentration in the solution decreases proportionally. A power-law dependence with a slope (exponent) of -1 is clearly seen in Fig. 2 for t_{str} as a function of C_{O_2} . This result could be rationalized having in mind that

$$t_{\text{str}} = \frac{q_{\text{UPD}}}{i_{\text{lim}}} \quad [2]$$

where q_{UPD} is the charge density of the UPD layer (constant) and for the sake of simplicity i_{lim} is assumed to be constant over the entire underpotential range. Now, combining Eq. 1 and 2 we get a mathematical expression for the inverse proportionality

$$t_{\text{str}} \sim \frac{1}{C_{\text{O}_2}} \quad [3]$$

This correlation explains the similarity between the OCP behavior in Pb/Ag(111) and Pb/Cu(111)¹⁰ systems. The experimental results obtained suggest the Pb monolayer as twice as stable on Ag(111) substrate. The latter finding is in perfect agreement with the reduction currents generated by a two-electron ORR on Pb-covered Ag(111)²⁰ vs four-electron ORR on Cu(111).²² These arguments identify the dissolved oxygen as a key oxidative agent that governs

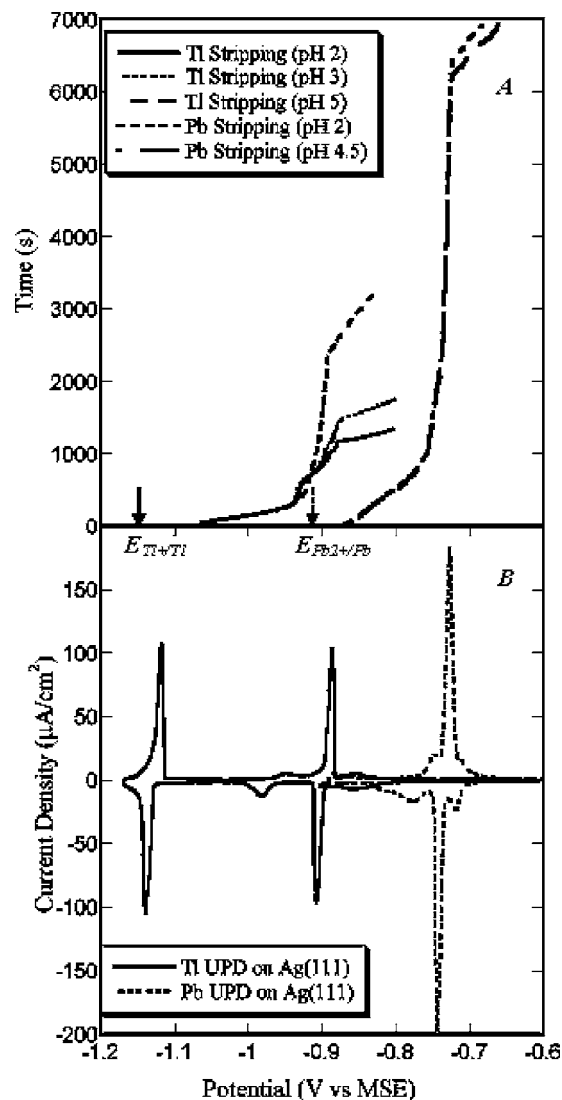


Figure 3. (A) OCP transients registered in the systems Pb/Ag(111) and Tl/Ag(111) in thoroughly deoxygenated 3×10^{-3} M $\text{Pb}(\text{ClO}_4)_2 + 1 \times 10^{-1}$ M NaClO_4 and 5×10^{-3} M $\text{TlClO}_4 + 1 \times 10^{-1}$ M NaClO_4 solutions, respectively, at different pH (as detailed in the legend). (B) Cyclic voltammograms of Pb/Ag(111) and Tl/Ag(111) processes in the above-mentioned solutions at pH = 2. Sweep rate 10 mV s^{-1} .

the stripping of Pb UPD layers in both systems at OCP.

The HER is another competitor to the metal ions in a galvanic displacement process. We demonstrated elsewhere¹⁰ based on kinetic data that HER cannot be considered as a major competitor in the case of Pb UPD layer stripping from Cu(111) electrode at OCP. In the present work a similar conclusion for the system Pb/Ag(111) can be illustrated by the identity of potential transients registered at pH 2 and 4.5 in solutions with the lowest possible oxygen concentration (Fig. 3A). It could be clearly seen that there is no significant change in the time for stripping a monolayer at OCP over more than two orders of magnitude difference in hydronium ions concentration. The latter argument, however, does not hold for the OCP behavior in the system Tl/Ag(111), where potential transients registered at pH 2, 3, and 5 in Tl^+ -containing solution with the lowest possible oxygen concentration show clearly a pH dependence (Fig. 3A). This result could be qualitatively explained. While the exchange current densities for HER on bulk Pb and Tl are of the same order of magnitude,²³ the HER overpotential would be about 250 mV more negative on Tl-covered Ag(111) in comparison with

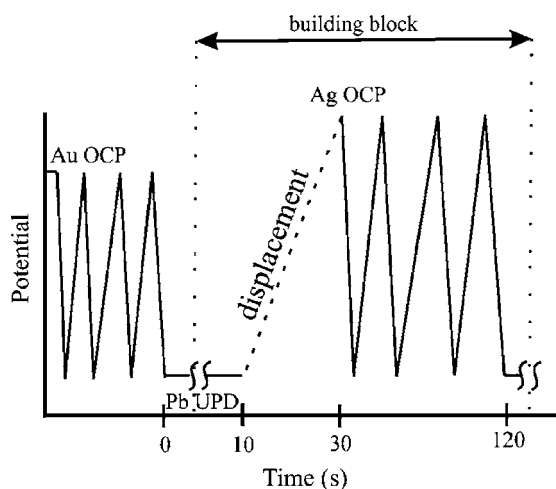


Figure 4. Schematic illustrating the time-potential protocol employed for a growth by galvanic displacement.

Pb-covered Ag(111) as determined by the equilibrium potentials of both metals (the arrows in Fig. 3). As a consequence a steady-state reduction current density, of -400 nA/cm^2 , is measured prior to potential transients at pH 2 in the system Tl/Ag(111) that is nearly ten times higher than the current density at the same pH for Pb/Ag(111) (-35 to -40 nA/cm^2). Wrapping up the above discussion, one needs to compare the potential transient registered for Tl UPD stripping at pH 5 with the one registered at pH 2 for Pb. In fact, such comparison clearly illustrates an identical rate of charge compensation in both cases taking into account the state of oxidation difference between Tl^+ and Pb^{2+} ions. This means that pH of Tl^+ solution needs to be as high as 5 so that the HER influence on the Tl UPD layer stability at OCP becomes negligible. In summary, the kinetic analysis suggests higher values of pH as more favorable for galvanic displacement-based protocols because of the negligible impact of HER on the UPD layer stability. However, in order to avoid any possibility for surface oxidation or hydrolysis we decided to perform our deposition experiments at pH 2, where even a Tl UPD layer would be stable for at least 300 s before any stripping is initiated (Fig. 3A).

Galvanic displacement of Pb monolayer.—The time-potential protocol employed for Ag deposition is schematically illustrated in Fig. 4. Before the deposition, the thermally reconstructed Au(111) surface (Fig. 5A) is subjected to a potential cycle in the Pb UPD range until a stable voltammogram, consistent with previous reports^{14,24} was registered (Fig. 6A). It has been shown that a Pb UPD layer lifts the thermal reconstruction,²⁵ thus populating the Au surface with highly mobile small clusters of atoms. A subsequent interaction between the relatively disordered Au surface and the Pb UPD layer leads to a surface alloying,¹⁴ eventually resulting in a morphology of Au(111) similar to the one presented in Fig. 5B. After the cycling, the Au surface was covered by a UPD layer of Pb and upon discontinuing the potential control it was transferred into a solution containing $1 \times 10^{-2} \text{ M Ag}^+$ ions. The optimal immersion time of 20 s to complete the stoichiometric redox exchange between Pb and Ag was established based on our kinetic study reported on in the previous paragraph. After the displacement, the surface was thoroughly rinsed by multiple immersions in deoxygenated water and transferred back to the Pb UPD cell where a cyclic voltammogram was registered (Fig. 6B). The peak potentials and shape of the curve in Fig. 6B are associated with the formation of a hexagonal close-packed monolayer of Pb on the Ag(111) surface.¹³ According to results of Pauling et al.,¹⁷ the remnants of features associated with Pb UPD on Au(111) suggest that less than two continuous MLs of Ag are present on the Au substrate. Apparently the Ag atoms cover

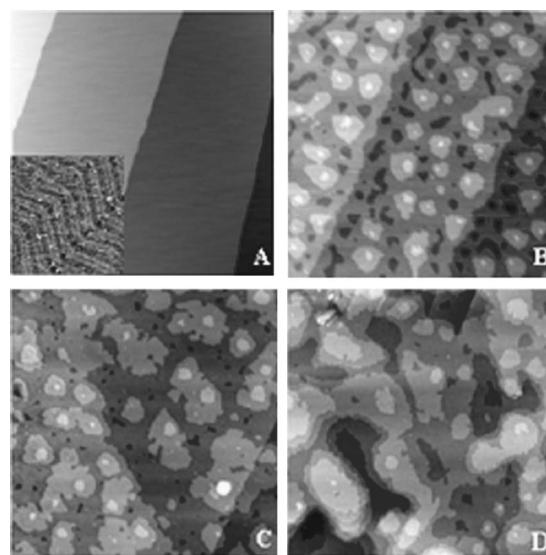


Figure 5. STM micrographs $570 \times 570 \text{ nm}$ illustrating: (A) thermally reconstructed Au(111) surface (inset size $60 \times 60 \text{ nm}$) and (B) the same surface after lifting of the reconstruction. Images (C) and (D) show the morphology evolution of the Ag layer with the thickness increase after 1 and 40 replacements, respectively.

the Au(111) surface uniformly as confirmed by the STM picture presented in Fig. 5C, where the overall morphology, clusters size, and average roughness are identical to those prior to the immersion experiment (Fig. 5B). A stripping experiment (not presented here) following the STM observation suggests the presence of about 1.7 Ag MLs on the Au surface in the case considered. According to Ref. 7, the amount of Ag atoms deposited in a single building block

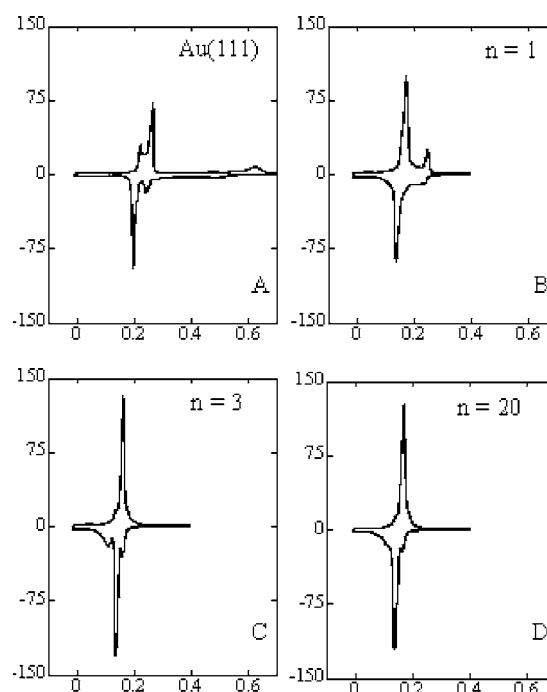
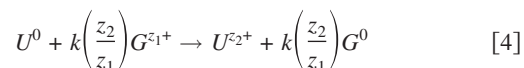


Figure 6. CV of bare and Ag-covered Au(111) surface after different number (n) of displacement cycles (A) $n = 0$; (B) $n = 1$; (C) $n = 3$; (D) $n = 20$ in $3 \times 10^{-3} \text{ M Pb}(\text{ClO}_4)_2 + 1 \times 10^{-2} \text{ M NaClO}_4$ (pH 2) solution. x axis: Underpotential (V); y -axis: current density ($\mu\text{A cm}^{-2}$). Sweep rate = 10 mV s^{-1} .

reaction upon 100% displacement efficiency (no side reactions taken into account) will depend upon the displacement reaction stoichiometry according to the following equation



where z_1 and z_2 are the oxidation states for the growing metal, G , and the UPD metal, U , ions, respectively. The coefficient $k = d_G/d_U$ is introduced in our previous work⁶ takes into account the different atomic densities, d (number of atoms per unit area), of G and U layers participating in the displacement reaction. Based upon grazing incidence X-ray scattering²⁶ and in situ STM results¹⁴ suggesting $d_{Pb} \approx d_{Tl}$ in the UPD systems $Pb^{2+}/Ag(111)$ and $Tl^+/Ag(111)$, respectively, the coefficient k should be within the range (0.74–0.79). These arguments set a theoretical limit of up to 1.6 MLs of Ag grown by a single displacement of a predeposited Pb UPD layer and up to 0.8 MLs of Ag when Tl is being displaced. The reason for obtaining a slightly higher amount of deposited silver (Eq. 4 predicts 1.6 MLs) is most likely associated with a deviation from the ideality for the system considered. Factors contributing to such behavior could be the surface roughness, inaccuracy of background current correction, edge effects, or tiny portion of Ag^+ ions introduced into the UPD cell after displacement. In general, despite these negligible differences, the building block procedure in our experiments is in excellent agreement with the findings of Brankovic et al. emphasizing a single-step Ag substrate modification by displacement of a Cu UPD layer.⁷

The new outcome that warrants the innovative aspect of our study is associated with a multiple application of the building block procedure for epitaxial metal growth. The galvanic displacement step described in the previous paragraph was repeated up to 20 times in the present study. The voltammetry curve displayed in Fig. 6C and 6D was registered on Ag layers grown by 3 and 20 displacements, respectively. The identical appearance of both curves with the curve registered on Ag(111) single-crystal (Fig. 3B-dashed line) suggests no qualitative difference in the surface morphology and energetics. This conclusion, providing no hints for 3D growth, is confirmed by the STM in Fig. 5D. Apparently, the surface morphology consists of atomically flat terraces 20–200 nm in size, separated by steps with monolayer height. A better justification for such statement could be found in Fig. 7 (with the corresponding voltammetry in Fig. 6C) that represents an intermediate morphology evolution registered after three displacement events. It is evident from the cross-sectional analysis in image A that the step height is always 1 atomic height. The higher resolution image C illustrates the (111) atomic structure of the topmost Ag layer, thus confirming the epitaxial growth in general. Also, the lower resolution image B sheds more light on the mechanism of growth associated with the displacement events. There is an apparent merging of clusters growing in a lateral direction (emphasized by the framed areas) that eventually leads to a layer completion. The lack of vacancy clusters deeper than 1 ML (Fig. 7, images A, B) and the relatively constant surface roughness after growth of 35 Ag layers suggests a quasi-perfect layer-by-layer growth mode.⁵

Galvanic displacement of Tl monolayer.—Thallium UPD on Ag(111) is among very few processes producing two monolayers in the underpotential range.^{27,28} A negative potential sweep results first in formation of one monolayer of underpotentially deposited thallium atoms on Ag(111) at underpotential of ~ 260 mV as shown in Fig. 3B, solid line. A continuing sweep gives rise to another deposition peak just before the equilibrium Tl/Tl^+ potential. Careful consideration of peak charges proves the association of most negative peak with the formation of the second Tl monolayer on Ag(111).^{27,28} Accordingly, two stripping peaks, respectively, associated with the corresponding monolayers appear when potential is swept in the positive direction (Fig. 3B, solid line).

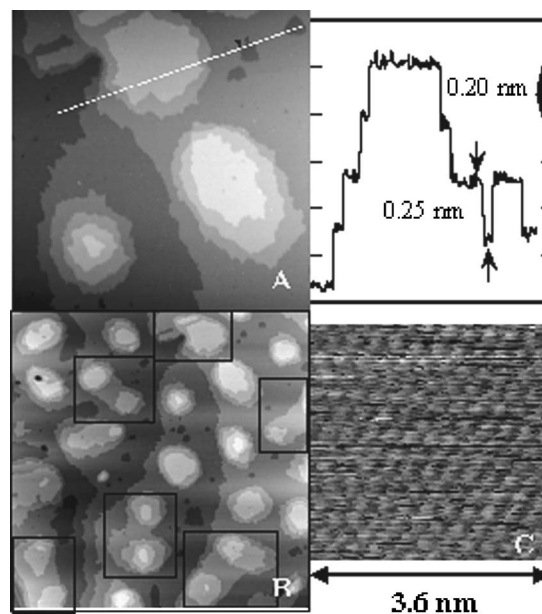


Figure 7. (A) STM image 320×320 nm with cross-sectional analysis illustrating the morphology evolution after three displacement events with five grown Ag layers. (B) STM image 700×700 nm providing clues for possible growth mechanism. (C) Higher resolution STM image 3.6×3.6 nm illustrating the (111) atomic structure of the topmost Ag layer.

The unique ability of Tl to form two monolayers on Ag(111) lends an opportunity to displace either one or two layers at once. For the purposes of this study we decided to investigate only one-to-one displacement. The cyclic voltammetry (CV) curves registered after different number of replacements are shown in Fig. 8. A careful

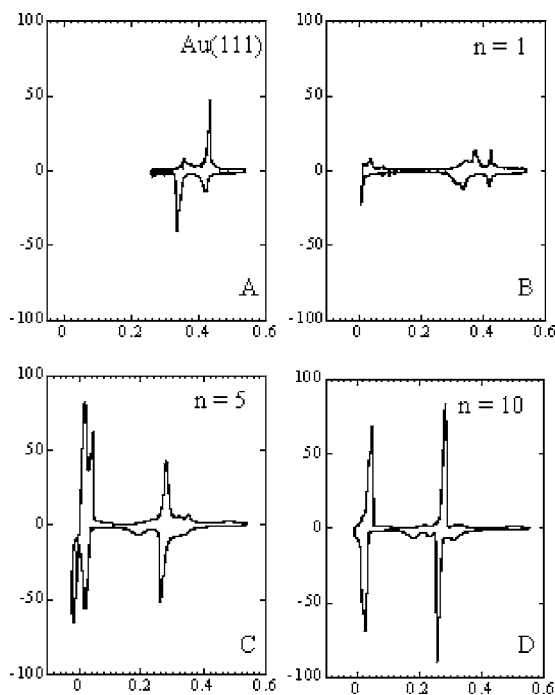


Figure 8. CV curves for Tl UPD on Au(111) and evolution of Tl UPD on Ag(111) after different number (n) of displacement cycles (A) $n = 0$; (B) $n = 1$; (C) $n = 5$; (D) $n = 10$ in 5×10^{-3} M $TlClO_4 + 1 \times 10^{-1}$ M $NaClO_4$ (pH 2) solution. x axis: Underpotential, (V); y axis: current density, ($\mu A cm^{-2}$). Sweep rate = $10 mV s^{-1}$.

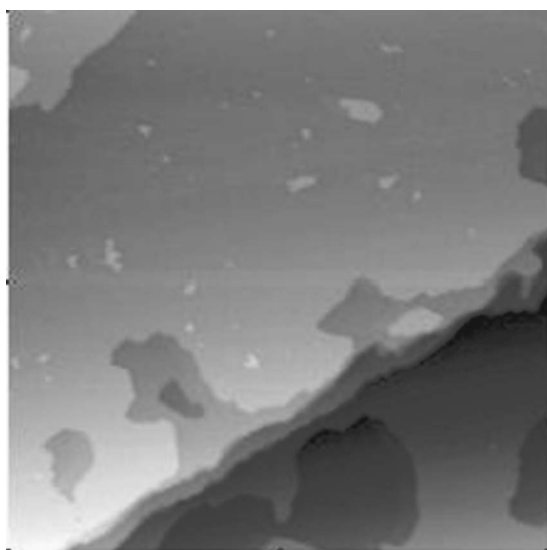


Figure 9. STM image of Au(111) surface after potential cycling in 5×10^{-3} M $\text{TiClO}_4 + 1 \times 10^{-1}$ M NaClO_4 (pH = 2) solution at a sweep rate of 10 mV s^{-1} . Scan size $750 \times 750 \text{ nm}$.

examination of the voltammetric features suggests a formation of at least two Ag layers uniformly spread on the gold surface after the fifth displacement.¹⁷ The Ag film acquires all properties of Ag(111) single crystal after the tenth displacement. Apparently, after this number of displacements, the whole crystal surface area acquires entirely the chemical potential of a bulk Ag(111).²⁹ All voltammograms in Fig. 8 are obtained right after the corresponding displacement event (without additional cycling also known as electrochemical annealing^{30,31}). However, a simple comparison suggests identical qualitative and similar quantitative (peak height and width) appearance of the CV curve obtained on as-deposited Ag film (after 10 displacements, Fig. 8D) with the one obtained on well-prepared Ag(111) single crystal (Fig. 3B, solid line). Having in mind that well-prepared Au(111) and Ag(111) surfaces feature average terrace sizes of 200 and 50 nm, respectively,^{32,33} the above-mentioned result rules out a substantial roughening and undoubtedly ascertains the quasi-perfect mode of growth during our deposition experiment.

The discussion of our STM results begins with an analysis of the Au(111) surface after a few successive deposition and stripping cycles of Tl UPD layer. Unlike the case of Pb UPD, where the voltammogram changed quantitatively with cycling, the current voltage curve in the presence of Tl demonstrated neither qualitative nor quantitative changes under identical circumstances. This result hints at substantially fewer changes taking place on the Au(111) surface in the presence of Tl and as a result on a flatter appearance (Fig. 9) after lifting of the thermal reconstruction of the Au(111) surface. In general, such behavior is not surprising, bearing in mind that no evidence for surface alloying in the system $\text{Tl}^+/\text{Au}(111)$ has been reported so far. In addition, the lack of alloying not only prevents the gold surface from roughening but also promotes the flattening and rearranging functions typical for successively deposited and stripped UPD layers.^{30,31}

Based on this reasoning, it can be expected that epitaxial growth of Ag on Au(111) assisted by galvanic displacement of Tl starts on initially flatter gold surface than in the case of GD of Pb. However, this does not necessarily mean that the initial roughness is the only factor contributing to the overall smoother appearance of the silver layer in the case of Tl GD (Fig. 9). As clearly illustrated by Fig. 10C, the first considerable morphological changes on the growing Ag surface could be seen after 20 displacement events corresponding to ~ 17 equivalent MLs (determined by integration of Ag stripping peak registered anodically of Ag OCP-Fig. 11). Before that the

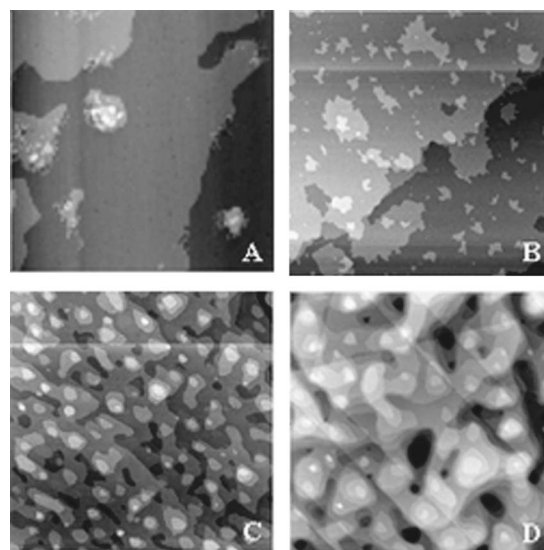


Figure 10. STM micrographs showing the morphology evolution with the thickness increase of Ag thin film on Au(111): (A) after 5 displacements; (B) after 10 displacements; (C) after 20 displacements; and (D) after 30 displacements. Scan size for all images is $750 \times 750 \text{ nm}$.

observed morphology (Fig. 10A and 10B) is almost identical to the one of the gold substrate (Fig. 9). In fact, a comparison with Fig. 7B of the present work strengthens this argument, as the morphology seen after 20 Tl GDs is quite similar to that observed after the third Pb GD. Apparently it takes less to initiate the process of surface roughening with using Pb as a displacement mediator.

Characterization by XPS.— The elemental composition of Ag films grown by galvanic displacement of Pb and Tl UPD layers was also analyzed. A two-point, depth-profile XPS analysis performed for both Pb (Fig. 12) and Tl (Fig. 13) with a limit of detection (LOD) 0.1 atom % found no traces of those metals incorporated into the deposit. This result is in concert with the elemental analysis of layers grown by DMG and SMG where traces of mediating metals were also not found.²⁻⁴ Indeed, the issue associated with surface alloying in $\text{Pb}/\text{Au}(111)$ ¹⁴ and $\text{Pb}/\text{Ag}(111)$ ^{34,35} systems is addressed

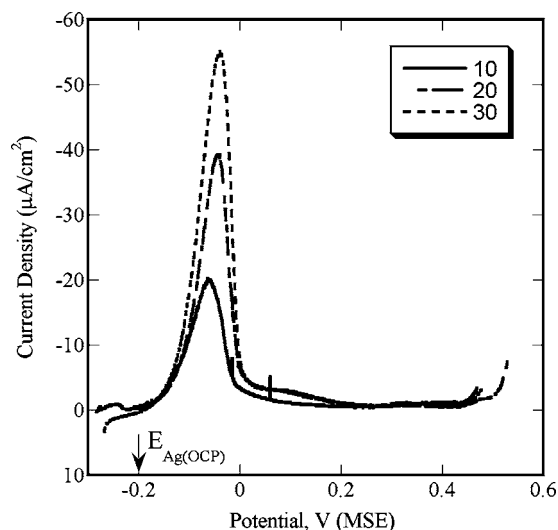


Figure 11. Anodic stripping voltammetry of Ag on Au(111) after n displacements (as detailed in the legend). Electrolyte: 5×10^{-3} M $\text{TiClO}_4 + 1 \times 10^{-1}$ M NaClO_4 , (pH 2); Sweep rate = 1 mV s^{-1} .

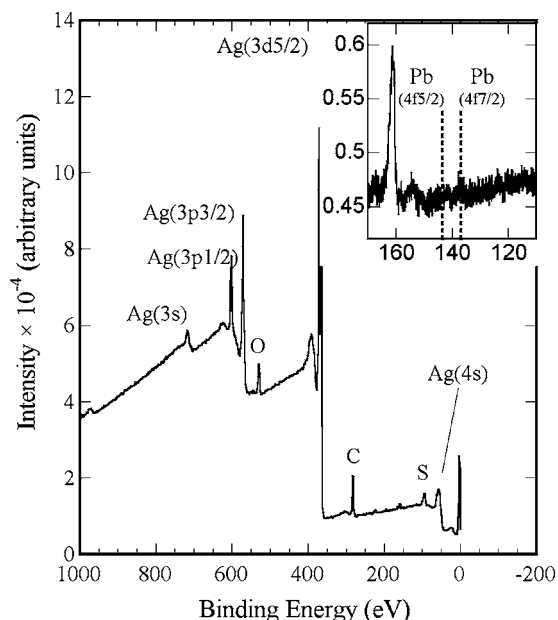


Figure 12. Characteristic XPS survey spectrum of 35 ML thick Ag layer grown on Au(111) by galvanic displacement of Pb UPD layer (main graph). The inset represents a high-resolution spectrum of the same sample where black markers indicate the expected peak positions presence of Pb exceeding 0.1 atom %.

by both (i) termination of the displacement step at a positive enough potential (the stability of a surface alloy depends upon the applied potential³⁵) and (ii) selection of parameters employed in the currently developed procedure that assume a fast displacement reaction (the surface alloying is typically a slow process³⁶). Such strict control makes virtually impossible the inclusion of any UPD metal participating in the displacement reaction provided there is a consider-

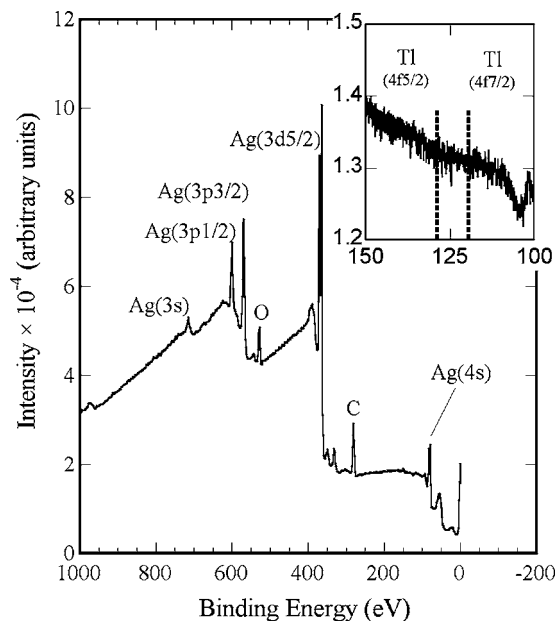


Figure 13. Characteristic XPS survey spectrum of 25 ML thick Ag layer grown on Au(111) by galvanic displacement of Tl UPD layer (main graph). The inset represents a high-resolution spectrum of the same sample where black markers indicate the expected peak positions presence of Tl exceeding 0.1 atom %.

able potential difference between the Nernst potential of the UPD metal and the corrosion potential of the growing metal.

Proposed mechanism of deposition by galvanic displacement.—

At present, a quantitative view of the monolayer restricted displacement mechanism is not available. However, well-known facts and the experimental results of this work allow for building a working hypothesis. The comparison of the above-described phenomenology should start with a description of the GD mechanism. According to our view, at a relatively high concentration (no diffusion limitations) of the displacing metal, its ions driven by the potential established by the UPD metal (Tl or Pb), first uniformly cover the predeposited UPD layer. Such flat layer deposition scenario satisfies the general requirement for lowering of the surface free energy as interpreted for a general UPD process in EC ALE⁹ and also following arguments explaining the surfactant mediation role of various UPD layers. Subsequently, a stoichiometric redox exchange, initialized mainly on the flat terraces, facilitates the formation of large clusters that grow laterally and eventually merge to yield a continuous epitaxial deposit. The flat terraces are identified here as displacement initialization centers because of the well-known fact that in a typical UPD system the stripping process always starts on terrace sites where the bonding to the substrate is weaker than on step and kink sites.^{13,29} Apparently the stoichiometric factor will be impacting the flux of the depositing metal in a single displacement event. Let us assume, for the sake of this argument, that every displacing atom will take the deposition site of the displaced one. Then, in the case of Tl, where displacing and displaced metals manifest equal state of oxidation (1:1), the odds for obtaining a layer that perfectly reproduces the substrate morphology are substantially higher. Following this general sequence of events in the case of Pb(2:1), there will be always an extra atom of Ag per displacement event with uncertain position in the growing layer. This extra atom will either occupy a spot next to its neighbor into the growing layer or will contribute to the nucleation of a second layer that takes place before the completion of the first one. Which of these two options takes place will also depend upon other factors such as stress accumulation, surface diffusivity, and energy to overcome the so-called Schwoebel's barrier.³⁷ A mathematical modeling and numerical simulations could help to quantitatively address this matter.

Conclusions

This paper reports on the development and experimental validation of a new method for growth of epitaxial metal films that utilizes a monolayer-restricted galvanic displacement as a building block reaction. A complementary kinetic study identifies ORR as a key oxidative competitor in the Pb displacement process, and both ORR and HER when Tl layer is subjected to galvanic displacement. Electrochemical and STM results illustrate a quasi-perfect, 2D growth of up to 35 ML of Ag on Au(111) assisted by repetitive galvanic displacement of a predeposited Tl and Pb UPD layers. The stoichiometry factor is found not only to control the film thickness but also to influence the morphology evolution of the growing Ag layer. An elemental analysis with LOD of 0.1 atom % suggests no traces of Pb or Tl in the accordingly deposited Ag layer.

Acknowledgments

The authors acknowledge that Fig. 4, 7, and 12 are also presented in Ref. 6 of this work. The authors thank Dr. Natasa Vasiljevic and Dr. Miomir Vukmirovic for the helpful discussion, Dr. Jonathan Shu from CNS at Cornell University for the assistance with the XPS measurements, and George Shovlowsky from SUNY Binghamton for the brilliant work in crafting the setup for controlled environment. The Research Foundation and IEEC at SUNY-Binghamton are gratefully acknowledged for the financial support of this work.

State University of New York at Binghamton assisted in meeting the publication costs of this article.

References

1. E. Bauer, *Z. Kristallogr.*, **110**, 372 (1958).
2. K. Sieradzki, S. R. Brankovic, and N. Dimitrov, *Science*, **284**, 138 (1999).
3. S. R. Brankovic, N. Dimitrov, and K. Sieradzki, *Electrochem. Solid-State Lett.*, **2**, 443 (1999).
4. S. Hwang, H. Oh, and J. Kwak, *J. Am. Chem. Soc.*, **123**, 7176 (2001).
5. J. X. Wang, B. M. Ocko, and R. R. Adzic, *Surf. Sci.*, **540**, 230 (2003).
6. R. Vasilic and N. Dimitrov, *Electrochem. Solid-State Lett.*, **8**, 173 (2005).
7. S. R. Brankovic, J. X. Wang, and R. R. Adzic, *Surf. Sci.*, **474**, L173 (2001).
8. J. L. Zhang, M. B. Vukmirovic, Y. Xu, M. Mavrikakis, and R. R. Adzic, *Angew. Chem., Int. Ed.*, **44**, 2132 (2005).
9. J. L. Stickney, *Electroanal. Chem.*, **75**, 25 (1999).
10. R. Vasilic, N. Vasiljevic, and N. Dimitrov, *J. Electroanal. Chem.*, **580**, 203 (2005).
11. S. G. Corcoran, G. S. Chakarova, and K. Sieradzki, *Phys. Rev. Lett.*, **71**, 1585 (1993).
12. E. Herrero, L. J. Buller, and H. D. Abruña, *Chem. Rev. (Washington, D.C.)*, **101**, 1897 (2001).
13. E. B. Budevski, G. T. Staikov, and W. J. Lorenz, *Electrochemical Phase Formation and Growth*, Wiley-VCH, Weinheim, Germany (1996).
14. M. P. Green and K. J. Hanson, *Surf. Sci. Lett.*, **259**, L743 (1991).
15. J. W. Schultze and D. Dickertmann, *Surf. Sci.*, **54**, 489 (1976).
16. I. Oh, A. A. Gewirth, and J. Kwak, *Langmuir*, **17**, 3704 (2001).
17. H. J. Pauling, G. Staikov, and K. Juttner, *J. Electroanal. Chem.*, **376**, 179 (1994).
18. S. Smolinski, P. Zelenay, and J. Sobkowski, *J. Electroanal. Chem.*, **442**, 41 (1998).
19. E. Herrero, J. Clavilier, J. M. Feliu, and A. Aldaz, *J. Electroanal. Chem.*, **410**, 125 (1996).
20. A. Zwetanova and K. Juttner, *J. Electroanal. Chem. Interfacial Electrochem.*, **119**, 149 (1981).
21. C. G. MacArthur, *J. Phys. Chem.*, **20**, 495 (1916).
22. G. Kokkinidis, *J. Electroanal. Chem. Interfacial Electrochem.*, **201**, 217 (1986).
23. O. A. Petrii and G. A. Tsirlina, *Electrochim. Acta*, **39**, 1739 (1994).
24. C. Chen, N. Washburn, and A. A. Gewirth, *J. Phys. Chem.*, **97**, 9754 (1993).
25. N. J. Tao, J. Pan, Y. Li, P. I. Oden, J. A. DeRose, and S. M. Lindsay, *Surf. Sci. Lett.*, **271**, L338 (1992).
26. M. F. Toney, J. G. Gordon, M. G. Samant, G. L. Borges, and O. R. Melroy, *J. Phys. Chem.*, **99**, 4733 (1995).
27. D. Carnal, P. I. Oden, U. Muller, E. Schmidt, and H. Siegenthaler, *Electrochim. Acta*, **40**, 1223 (1995).
28. H. Siegenthaler, K. Juttner, E. Schmidt, and W. J. Lorenz, *Electrochim. Acta*, **23**, 1009 (1978).
29. I. V. Markov, *Crystal Growth for Beginners: Fundamentals of Nucleation, Crystal Growth and Epitaxy*, World Scientific Publishing Co. Inc., Singapore (1995).
30. D. M. Kolb, *Prog. Surf. Sci.*, **2**, 109 (1996).
31. L. G. Goetting, B. M. Huang, T. E. Lister, and J. L. Stickney, *Electrochim. Acta*, **40**, 143 (1995).
32. M. H. Holzle, V. Zwing, and D. M. Kolb, *Electrochim. Acta*, **40**, 1237 (1995).
33. W. Obretenov, U. Schmidt, W. J. Lorenz, G. Staikov, E. Budevski, D. Carnal, U. Muller, H. Siegenthaler, and E. Schmidt, *J. Electrochem. Soc.*, **140**, 692 (1993).
34. T. Vitanov, A. Popov, G. Staikov, E. Budevski, W. J. Lorenz, and E. Schmidt, *Electrochim. Acta*, **31**, 981 (1986).
35. N. Dimitrov, A. Popov, T. Vitanov, and E. Budevski, *Electrochim. Acta*, **36**, 2077 (1991).
36. A. Popov, D. Kashchiev, N. Dimitrov, and T. Vitanov, *J. Cryst. Growth*, **171**, 250 (1997).
37. R. L. Schwoebel and E. J. Shipsey, *J. Appl. Phys.*, **37**, 3682 (1966).